IEEE Access
Multidisciplinary | Rapid Review | Open Access Journal

Received September 21, 2020, accepted October 9, 2020, date of publication November 16, 2020,
date of current version November 25, 2020.

Digital Object Identifier 10.1109/ACCESS.2020.3037450

Robust Breast Cancer Imaging Based on a Hybrid Artifact Suppression Method for Early-Stage Tumor Detection

MEHDI MEHRANPOUR[1], SAUGHAR JARCHI[1], (Member, IEEE), ASGHAR KESHTKAR[1], AYAZ GHORBANI[2], ALI ARAGHI[3], (Graduate Student Member, IEEE), OKAN YURDUSEVEN[4], (Senior Member, IEEE), AND MOHSEN KHALILY[3], (Senior Member, IEEE)

[1]Faculty of Technical and Engineering, Imam Khomeini International University, Qazvin 34149-16818, Iran
[2]Department of Electrical and Electronic Engineering, Amirkabir University of Technology, Tehran 15916-34311, Iran
[3]Home of the 5G Innovation Centre (5GIC), Institute for Communication Systems (ICS), University of Surrey, Guildford GU2 7XH, U.K.
[4]School of Electronics, Electrical Engineering and Computer Science, Institute of Electronics, Communications & Information Technology, Queen's University Belfast, Belfast BT7 1NN, U.K.

Corresponding author: Ali Araghi (a.araghi@surrey.ac.uk)

ABSTRACT a high-resolution conformal array for detection of small size tumors inside the breast is proposed. The array consists of a novel cavity-backed low-profile aperture-stacked-patch (LP-ASP) antennas. The proposed antenna operates from 2.2 GHz to 13.5 GHz which enables the imaging system to be exploited across a high fractional bandwidth of approximately 149%. Thanks to the wide operating bandwidth of the designed antenna, the proposed system is not only applicable for a deep penetration imaging, but also for high resolution and accurate images acquisition. The proposed single element antenna has a compact size of $10 \times 10 \times 10.495\text{mm}^3$. So, it is possible to form a conformal array around the breast by applying numbers of the designed elements. Moreover, a Hybrid Artifact Suppression (HAS) method is presented to remove the artifact effects including skin reflection and mutual coupling between the elements. In this method, the artifact response of each channel is estimated using Independent Component Analysis (ICA) at the early-stage of the recorded signals. Additionally, in order to suppress the artifact data to accurately detect the malignant tumor, a Wiener filter is applied. To validate the practicality of the presented calibration algorithm in the proposed conformal array, the detection of a single spherical tumor (with a small diameter of 5 mm) within a realistic breast model in different scenarios is studied. Investigating of simulated and measured results of the designed antenna, and comparing quantitative metrics of successfully reconstructed tumor images by the proposed HAS and conventional calibration methods show the proposed system can be a good candidate for the breast cancer detection applications.

INDEX TERMS Cavity-backed antenna, aperture-stacked-patch (ASP) antenna, microwave imaging, breast cancer, artifact removal (AR) algorithm, high-accuracy calibration method, confocal microwave imaging algorithm, independent component analysis (ICA), focal points, conformal array.

I. INTRODUCTION

Breast cancer is a group of diseases that has been concern in women worldwide. This type of cancer cells eventually from a lump or mass called a tumor, and typically produces no symptoms when the tumor is small and most easily treated. Thus early-stage detection before symptoms are developed is recognized as the most effective treatment as there is no way to prevent the breast cancer [1] One of the most common methods in breast screening for early detection of cancer is X-ray mammography.

Ionizing radiation, detection failure, low contrast, and uncomfortability are of the most irritating issues during the X-ray mammography for breast cancer detection [2], [3]. Consequently, microwave imaging systems are mainly emerged to remove the aforementioned limitations for early breast cancer detection [4]. In general, there are two types of microwave imaging systems: Microwave Radar-based (MR),

The associate editor coordinating the review of this manuscript and approving it for publication was Kai-Da Xu.

and Microwave Tomography-based (MT). In the MT imaging, localizing and detection of the breast cancerous tissues is performed by solving a forward and reverse scattered field problem through analyzing the received scattered waves [5]. In the MR imaging, an antenna (or an array of antennas) is applied to transmit and receive ultra-wideband (UWB) pulses by employing the transmitter (Tx) and the receiver (Rx) antennas in different locations [4]. The information about the target's position and size can be obtained by calculation of the time delay between the transmitted and received signals, with the aid of assessing the amplitude of the received signals. Instead of reconstructing the full electrical profile of the imaging area in the MT, the MR can detect and localize present tissues with high scattered signals only. As a result, the MR imaging is less computationally complex and time-consuming than the MT [6].

Data acquisition systems within the microwave imaging can be divided into three categories: monostatic, bi-static, and multi-static. In monostatic imaging systems, transmitting and receiving data are carried out using the same antenna, which can be placed in different positions over the breast or fixed as an element of an antenna array [7]–[10]. For bi-static case, each element of a fixed-element array illuminates the breast sequentially while the other antennas as Rx elements record scattering at different angels from Tx boresight. In multi-static systems, both the obtained monostatic and bi-static data are taken into account for imaging [11], [12]. Due to a higher number of Tx-Rx channels, and the various recorded scattering angels upon each transmission, a considerable amount of data can be acquired in the last approach compared to the two other categories [7]–[12].

The recorded signal of each channel contains skin, intra-element coupling, and internal breast tissue responses. Generally, the skin response can be significant and take place at an earlier time because of the higher electrical properties than other tissues and the closer distance to Rx, which generates an artifact and multi- reflections at the early-time of the recorded signal which must be suppressed [13], [14]. The skin artifacts removal is called calibration processing. Various calibration methods have been investigated within the MR imaging lectures previously. The simplest calibration method also known as ideal calibration, carried out by subtracting the recorded signals without tumor from the breast model with tumor [15]. Since a priori knowledge from the tumor-free breast is not normally available, the ideal calibration is not practical. Therefore, practical calibration methods have been investigated recently [16]–[25]. The averaging method was proposed in [16], which the artifact calibration is employed by subtracting the received signal in one channel from the average of other channels. In order to compensate the channel-to-channel signal variations in the [16], the woody averaging was proposed in [17]. Compared to the normal averaging method, this method applies additional preprocessing which is alignment based on the cross-correlation [18]. The differential rotation method was presented in [19] and to eliminate the artifacts, the first data subtracted by dataset which acquired by a specific-angle rotated array. The average subtraction method can be improved by using the Wiener filter algorithm, which requires information about the skin time location [7] and [20]. Based on updating filter weights, a different type of filter is called the root least squares (RLS) filters was presented in [21]. The neighborhood-based algorithm was proposed in [22]. In this method, the skin response at a given antenna is filtered using the skin reflections are measured at neighboring antennas. In [23], the differential method was presented. In this approach, the recorded signals from two successive scans are compared and the effects of changes in the scanning environment are mitigated by a Support Vector Machine (SVM) classification algorithm. In [24], the entropy-based time widowing (ETW) method was proposed to remove the skin reflections by using of their similarity of artifacts across the channels. The hybrid artifact removal (HAR) methods using both Wiener filter and ETW algorithms were introduced in [25], [26]. Additionally, the independent component analysis (ICA) method by increasing the measured data based on the repositioning of the fixed-antenna array was presented in [27]. In the mentioned method, the artifact effect is removed by subtracting the ICA estimated skin from the received signals. Finally to construct the images, reconstruction algorithms such as data-dependent or data-independent Rx beamforming are required to be applied on the calibrated signals [28]–[31].

In general, the most important issues to design a succesful calibration method are

- The estimation of the skin effect in the early-stage of recorded signals with high precision.
- The compensation of the channel to channel variation in transmission channels.
- The suppression of the artifacts more efficiently.
- The extraction of the mixed tumor response in the late-stage of recorded signals with high accuracy.

However, several operational microwave breast cancer imaging systems have been introduced by different research groups. In this paper, eight most important systems are reviewed [32]–[34]. The first system was developed at Dartmouth College, USA (DC) in 2000 [35]. This system has been designed based on MT imaging and applied in a number of 150 clinical trials to date [36], [37]. After that, the Multistatic Array Processing for Radio Image Acquisition (MARIA) system using radar-based imaging was presented at the University of Bristol, UK [38]. The system is now being commercially developed by Micrima Ltd., Bristol, UK and has been examined with 223 patients to date [39], [40]. In 2013, the Tissue Sensing Adaptive Radar (TSAR) system based on MR imaging was developed at the University of Calgary, CA that has been used with 8 patients [8], [41]. A wearable and a table-based MR imaging system were presented by researchers at McGill University, Canada (MU) in 2016 [42], [43]. The table-based and wearable systems have been tested with 13 and 38 healthy women, respectively in a clinical trial. In 2017, an MR imaging system

was presented at the Southern University of Science and Technology, China (SUST) [44]. To date, clinical trial results with 11 Asian women have been presented from Phase I of the mentioned system. In the same year, a handheld MR imaging system was developed at Hiroshima University, Japan (HU) that has been examined with five women with disease [45]. Also, an operational system based on MR imaging was developed at Shizuoka University, Japan (SU) in 2017 [46]. In the SU system, three different sensor types were designed using 6, 18 and 30 antenna array for various breast sizes that have been tested with 2 patients to date. Finally, in 2018, early reports from an ongoing clinical study at the Clinical Research Facility of Galway University Hospital (CRFG) by Microwave Vision Group (MVG) was reported [47]. The Wavelia MR-based imaging system is a low-power electromagnetic wave operational system, which consists of two subsystems: A Microwave Breast Imaging (MBI) subsystem and an Optical Breast Contour Detection (OBCD) subsystem [48]. In this system, a circular antenna array is applied to scan the breast and a new shape-based calibration method integrating with the OBCD subsystem has been developed to compute the breast volume. The MVG is engaged in active clinical trials with 30 tumor patients whose results are expected by the end of 2020 [49]. To date, the Wavelia system has been exanimated on 20 patients in total. However, a significant difference in design exists between the microwave systems in terms of prototype and data acquisition systems, patient interface, the calibration algorithms, and the image reconstruction techniques. Although the majority of the mentioned systems use a table-based prototype while the patient is laid in a prone position on the top of the table (e.g. DC, MARIA, TSAR, SUST, SU, and Wavelia), some have been designed without using an examination table while the patient is laid in a supine position (e.g. HU) or is placed in a seated position (e.g. MU). Additionally, in some of these systems the breast is immersed into a coupling/matching medium during scanning time to ease the wave propagation inside of the breast tissues (e.g. DC, TSAR, SUST, and Wavelia), while in some is applied a solid coupling shell and the patient's breast is contacted directly to the shell (e.g. MARIA, MU, HU and SU). In two of these systems (HU and MU), no coupling medium has been demonstrated [32]–[34]. The features of the reviewed system are summarized in Table 1. Among the existing operational systems, the MARIA system has been more successful due to much less scan time (less than 1 minute), the largest trials and its exceptional sensitivity [32], [50]. Recently, this system has been installed in hospitals in Austria and Switzerland by Hologic Inc. (a global leader in woman health) [50].

Various antenna types have been applied in the operational systems. In DC system, 16 monopole antennas were applied as the elements of a circular array [35]. In Micrima Ltd., they developed a hemispherical antenna array using 60 wide-slot antennas for the last version of MARIA system [40]. In previous version, they applied a hemispherical antenna array consisting of 16 aperture stacked patch (ASP) antennas [28]. Both the wide-slot and ASP antennas operate in the frequency range of 4-8 GHz while the size of wide-slot antenna (14×13 mm^2) is 3 times smaller (in terms of front face) than that of the ASP antenna (18×18 mm^2) [51]. TSAR's group applied an antipodal Vivaldi antenna with the size of 80×44 mm^2 operating over the frequency range from 1.3 to 7.6 GHz for their system [8], [52]. In MU systems, they developed a flexible microstrip and a TWTLTL antennas for the wearable and table-based prototypes, respectively [42], [43]. The antenna array was made of 16 elements in both systems while the size of the flexible and TWTLTL were 18×18 mm^2 and $12 \times 15.8 \times 0.635$ mm^3, respectively. The mentioned antennas have been designed to be operated in the range of 2-4 GHz. In SUST, a horn antenna with an aperture size of 20×20 mm^2 operating in the range of 4-8.5 GHz was developed for a visual array system [44]. In the HU, they applied a planar slot antenna with a size of $11 \times 13.1 \times 0.635$ mm^3 as the elements of the multistatic antenna array containing 16 elements [45]. The applied antenna operates in the range of 3.1-10.6 GHz and is a modified version of the designed antenna in [53]. SU's group designed a stacked patch antenna for their system. The proposed antenna operates from 4 GHz to 9 GHz by embedding in the coupling shell [46]. In the Wavelia system, the MVG applied a network of 18 Vivaldi antennas with the operating frequency range of 1-4 GHz in a horizontal circular configuration [47].

In addition to the discussed antennas in the mentioned operational systems, several antennas (which are capable to be applied in the breast cancer detection applications) have been proposed. In [54], an ASP antenna with a patch size of 6.5×9 mm^2 was proposed to radiate directly into a breast model in the frequency range of 4-9.5 GHz. Unlike its compact patch, the overall size of the antenna is still bulky due to its feeding line. A tapered slot antenna with a size of 19×19 mm^2 was proposed in [55] which is analogous to the antenna setup in [54]. The performance of the designed antenna was experimentally validated on a breast phantom. The results showed that the antenna has a bandwidth from 2 GHz to 8 GHz. In [56], a horn antenna with an aperture size of 61.6×61.6 mm^2 was designed for the breast cancer imaging applications. The antenna has been designed to be operated in the frequency range of 1.5-6 GHz inside of Canola oil. A modified bowtie antenna with a size of 15×15 mm^2 and the reflection coefficient below -8 dB to operate in the frequency range of 1.2-7 GHz inside of a polyethylene glycol-water solution was presented in [57]. In addition to the mentioned antennas that have been designed in a way to work in a coupling medium or contact directly to the skin tissue during breast scanning (e.g. [54]–[57]), several air-coupled antennas have been introduced in the literatures [58]–[60]. In these types of antennas, since it usually is required to suppress strong reflection from the breast-air interface, the antennas are designed in larger sizes and higher gain compared to the previous antennas [32]–[34], [61]. Design of a compact size antenna enables us to have large number of elements in a dense array while, at the same time, will decrease the

volume of the imaging system, and consequently the elements of the array can be placed close to a target object and more data could be captured [32]–[34]. Besides, having an antenna covering both lower and higher frequencies around UWB frequency range to guarantee high resolution as well as good penetration into the breast tissues is another important challenge [33]. Therefore, limited broadband characteristic and large size are the major trade-off associated with the antennas. To the best of author's knowledge, the majority of the current breast cancer imaging procedures are performed using the planar-type antennas due to their simple structure, compact size, broadband properties, and ease-to-fabricate. Among the planar-type antenna elements, the ASP antennas show promising results in terms of impedance matching, wide beamwidth to encompass a sensible portion of the breast, and consistent radiation patterns [28], [54].

This paper presents a robust breast cancer imaging system with a new calibration algorithm to extremely suppress the artifact effects. As it has been described in [27], non-uniform skin contours can diminish the performance of the MR imaging methods. Also in [38], the authors have highlighted the difficulties when the skin is not a smooth uniform contour using the differential rotation method. Therefore, a breast model with a varying skin thickness range from 1 to 3 mm is investigated in the designed system. In order to remove the skin effect, a Hybrid Artifact Suppression (HAS) method is proposed. In this algorithm, Wiener filter is applied to reduce the artifact effects extremely, rather than subtracting the estimated skin signal from the original one as is employed in the conventional ICA [27]. It must be noted that the calibrated signals that are obtained by Wiener filter often do not perform well for the recorded multi-static data from the mentioned non-uniform skin breast phantom where the tumor responses are filtered out in some channels. On the other hand, the artifacts are not removed efficiently using the Woody averaging method although the tumor responses are estimated property [27]. Therefore, an additional pre-processing through cross-correlation analysis between the Woody averaging and Wiener filter data is investigated and presented in this paper. The performance of the proposed HAS algorithm is validated using a novel cavity-backed low-profile ASP (LP-ASP) antenna to detect a small tumor for two difficult scenarios (near the skin tissue and on the axis of rotation). The proposed cavity-backed LP-ASP antenna consists of a modified coupling aperture (attached H-shaped and Cross-shaped slots) and a fork-shaped feeding structure which benefits from proper multi-layer substrates. To evaluate the practicality of the presented antenna based on the prototype in [40], the antenna is immersed in a matching liquid similar to normal breast tissues and hence achieves a fractional bandwidth of approximately 149% (2.2-13.5 GHz). To the best of our knowledge, the proposed antenna has the smallest size (in terms of front face) with the widest bandwidth among the reported previous antennas. Therefore, the applied array can be densely populated around the breast model. Besides, compared to the wide-slot and conventional

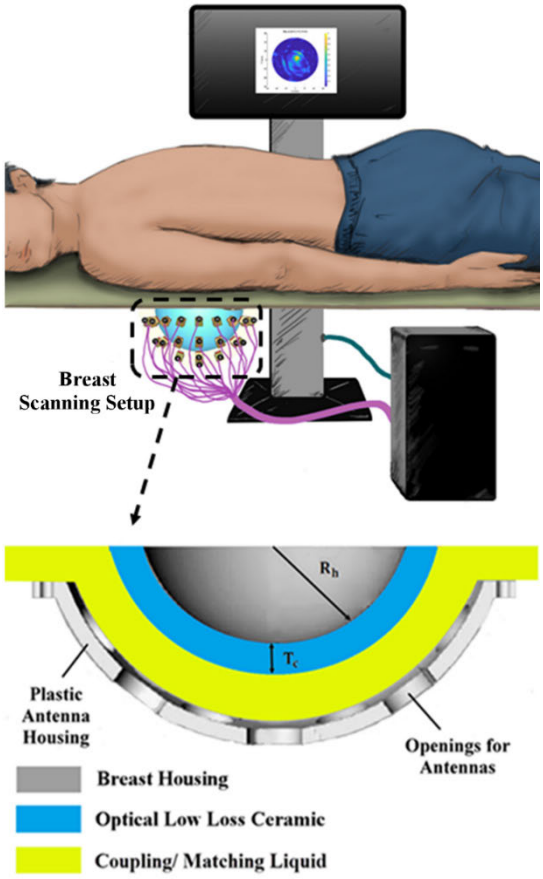

FIGURE 1. The scanning setup for the proposed breast imaging system which is inspired by that of presented in [19], [62].

ASP antennas used in the previous arrays [40], [28], the proposed LP-ASP antenna includes both lower and higher frequencies to have a good penetration as well as high resolution features for the breast cancer detection applications.

This paper is organized as follow; in Section II, the proposed breast cancer imaging system and the antenna array configuration will be presented. The details of the proposed skin calibration method will be detailed and discussed in Section III. Section IV investigates the examining results of the designed microwave imaging system; following by the conclusion in Section V.

II. PROPOSED MICROWAVE IMAGING SYSTEM

The microwave imaging system setup in this work is shown in Fig. 1 which is inspired by that of presented in [19], [62]. In this system, a table-based prototype is applied for a patient who laid down in a prone position while her breast is inserted into a hemispherical cup. In this setup, first, the antenna elements of a hemispherical array are immersed into a coupling/matching medium/liquid to reduce the reflection of transmitted signals from the skin-air interface to ease the wave propagation inside the breast tissues. Then, a hemispherical-shell ceramic is used to accommodate a cup with size of the breast which is placed on top of the matching

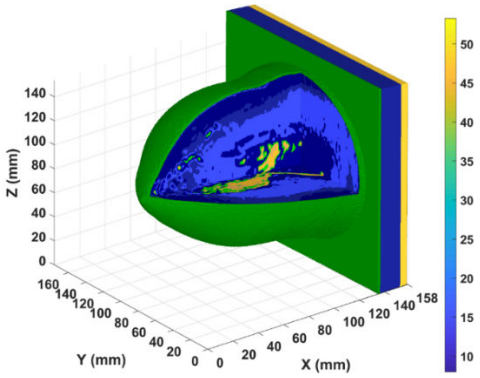

FIGURE 2. The MRI-derived scattered fibroglandular breast model at 4.5 GHz.

medium. Finally, before the insertion of the phantom into the mentioned ceramic, a small amount of the matching liquid is applied to ensure that no air gaps are remained.

A. THE BREAST MODEL

In this system, a breast model with a non-uniform skin thickness (varying from 1 to 3 mm), which agrees with reported results in [63], [64] is employed in the proposed microwave imaging system. In order to create such model, the MRI-derived anatomically breast model (ACR class II) from the University of Wisconsin-Madison MRI breast cancer repository is applied as a basic breast phantom [65]. The ACR class II breast model consists of $316 \times 352 \times 307$ cubic voxels having a small voxel size of $0.5 \times 0.5 \times 0.5$ mm^3. This MRI-derived breast model is composed of several layers as are listed below [65]:

- a roughly 1.5 mm thick skin layer at both breast and pectoral regions.
- a 1.5 cm thick subcutaneous fat layer at the base of the breast.
- a 0.5 cm thick muscle chest wall at the pectoral region.

which is classified as scattered fibroglandular breast model regarding 25-50% glandular tissue density at the base of breast. The mentioned breast model is shown in Fig. 2 at 4.5 GHz, while the colorbar displaying the relative permittivity of each tissue.

Suppose that the mentioned breast model is fitted into the hemispherical breast housing (see Fig. 1) during the scanning, therefore, it is required that the model mapped to a hemispherical profile as is performed in the realistic environment [29]. To realize this fibroglandular breast phantom with the mentioned non-uniform skin thickness, first, the 3D CAD models of the skin layer and internal environment of the desired phantom at the base of the breast region are sketched in a CAD modeling software such as Autodesk 3ds Max [66] as shown in Fig. 3 (a), then, the CAD models are imported into MATLAB [67], next, the calculated electrical properties using a single-pole Debye model [14] for the ACR class II breast tissues [65] are interpolated at the points are placed inside of the CAD data of the modified breast model, finally, two ASCII text files, *mtype.txt* and *pval.txt*, providing tissue

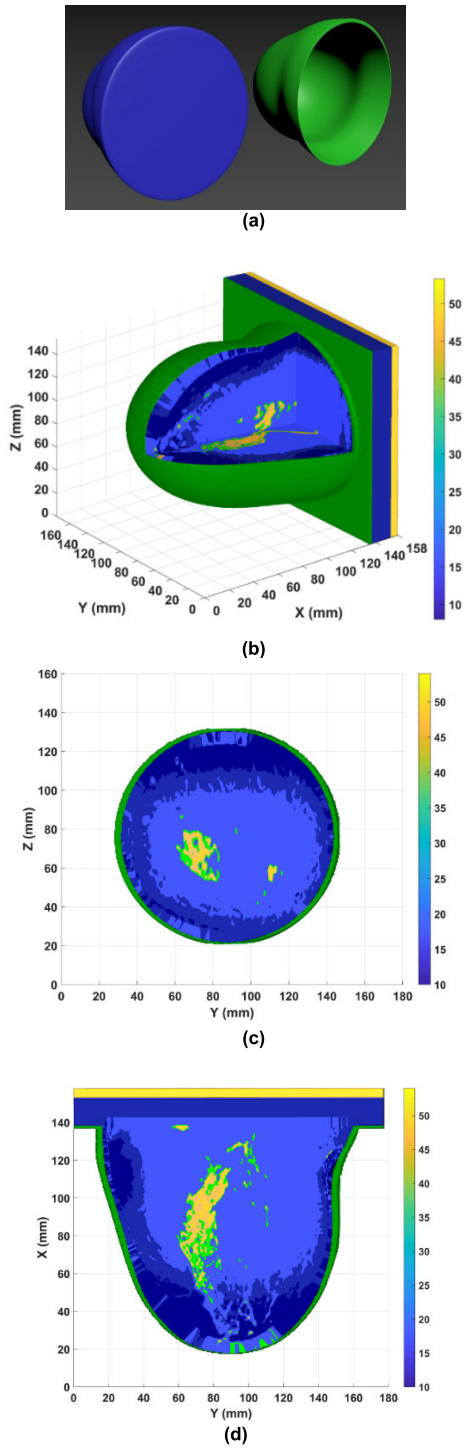

FIGURE 3. (a) The 3D CAD models for the internal environment (left) and skin layer (right) of a breast phantom with a non-uniform skin thickness (varying from 1 to 3 mm) which is mapped to a hemispherical profile (b) The 3D profile of the modified breast model at 4.5 GHz, (c) The modified breast model at X = 77 mm slice plane, (d) The modified breast model at Z = 73 mm slice plane.

type (particular number) and dielectric properties information for each voxel in the modified breast model are generated. It must be noted that the points are located within the CAD models determined by data processing of generated mesh cells on the imported CAD models in MATLAB.

TABLE 1. The features of the reviewed operational breast cancer detection systems.

	DC [35]	MARIA [40]	TSAR [41]	MU (Table-Based) [42]	MU (Wearable) [43]	SUST [44]	HU [45]	SU [46]	Wavelia [47]
Patients (Largest Trials)	150	223	8	13	38	11	5	2	pilot
Scan Time	5 min	10 s	30 min	18 min	5 min	4 min	14 min	3 min	10 min
Imaging System	MT	MR	MR	MR	MR	MR	MR	MR	MR
Coupling	medium	shell	medium	medium	shell	medium	shell	shell	medium
Data Acquisition	multistatic	multistatic	monostatic	multistatic	multistatic	multistatic	multistatic	multistatic	multistatic
Operating Freq. (GHz)	0.7-1.7	4-8	1.3-7.6	2-4	2-4	4-8.5	3.1-10.6	4-9	1-4
Calibration Method	-	differential rotation	neighborhood-based	differential	differential	Wiener filter	averaging	differential rotation	A new shape-based

Consequently, in order to construct the modified breast model in CST microwave studio simulator [68], first, a 3D structural data of the breast tissues regarding the generated particular number (*mtype.txt*) of each tissue at the points of the CAD model is created, then, a corresponding binary or material file which contains the dielectric properties of all tissues in the modified breast model is built. Finally, to import the 3D structural data into CST software, a voxel file for the modified breast model is created. The voxel file contains the information about the dimension of the model which is linked to the structural and material files. The 3D profile of the modified breast model at 4.5 GHz is illustrated in Fig. 3 (a), while Figs. 3 (b) and (c) show the model at X = 77 mm and Z = 73 mm slice planes.

B. CAVITY BACKED LP-ASP ANTENNA

A detailed image of the proposed cavity-backed LP-ASP antenna is illustrated in Fig. 4. As shown in the figure, the antenna is embodied by three substrates: Sub_1 (Rogers RT/duroid 6010 with thickness 0.635 mm), Sub_2 (Rogers RT/duroid 5880 with thickness 1.57 mm), and Sub_3 (Rogers RT/duroid 6010 with thickness 1.27 mm). Also it can be seen from the figure, the proposed antenna consists of a modified coupling aperture (the attached Cross and H-shaped slots) and a fork-shaped feeding structure, which two rectangular patches with the same size of ($W_p \times L_p$ =) 6 × 3 mm^2 are stacked up on the topside of Sub_2 and Sub_3. The other optimal parameters of the proposed antenna are: W_{sub} = 10 mm, L_{sub} = 8.5 mm, h_u = 1.27 mm, h_l = 1.57 mm, h_f = 0.635 mm, L_f = 4 mm, F_s = 3 mm, L_s = 1.85 mm, L_h = 5.75 mm, W_h = 9.5 mm, Q_s = 4.25 mm, Q_p = 4.25 mm, W = 0.7 mm, L = 1.5 mm, L_a = 1.5 mm, W_a = 0.5 mm, W_c = 1.2 mm, L_c = 0.5 mm, and L_{sma} = 1.5 mm.

In order to suppress the back-lobe, a cavity is used at the back of the LP-ASP antenna as shown in Fig. 4 (c). Besides, to absorb the additional resonances, the interior of the cavity's faces is filled by a broadband absorbing material (Eccosorb FGM-40) with a thickness of W_{ab} = 1.02 mm, which is spaced L_{air} = 6 mm from the top surface of feeding structure. Two prototypes of the fabricated cavity-backed LP-ASP antenna is shown in Fig. 4 (d).

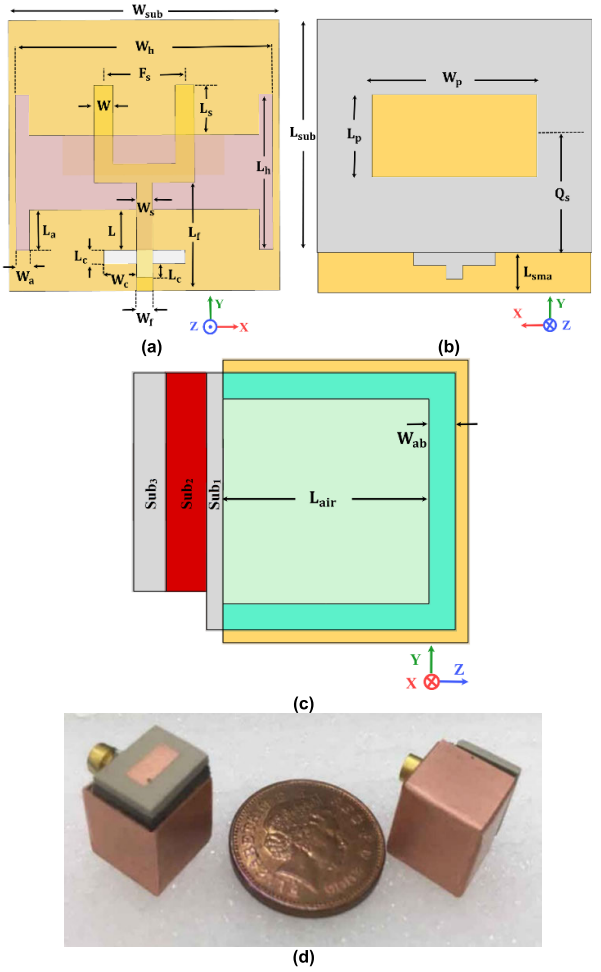

FIGURE 4. The proposed cavity-backed LP-ASP antenna (a) Top view (b) (b) Bottom view, (c) Side view (d) The fabricated cavity-backed LP-ASP antennas.

C. ANTENNA PERFORMANCE/CHARACTERISTICS

In order to validate the usefulness of the cavity-backed LP-ASP antenna in the proposed microwave imaging system,

the antenna should be immersed in a coupling medium as was mentioned previously. The coupling medium in this system is a dispersive liquid with a dielectric constant of $\boldsymbol{\varepsilon_r = 9}$ and a static conductivity of $\boldsymbol{\sigma = 0.4}$ S/m at 7 GHz. In the laboratory environment, we made such liquid by a mixture of distilled water, paraffin oil, and beeswax (while the last one is applied as an emulsifying agent) according to the procedure has been described in [69]. During measuring the characteristics of the antenna, the antenna is immersed into the provided liquid as shown in Fig. 5 (a). The simulated and measured characteristics of the proposed antenna in the coupling medium are illustrated in Figs. 5 (b) and (c). In the simulation environment, a dispersive single-pole Debye model is applied to represent the coupling medium. As shown in Fig. 5 (b), the proposed antenna operates in the frequency range of 2.2 to 13.5 GHz when $|\boldsymbol{S_{11}}| \leq \boldsymbol{-10\ dB}$. Besides, Fig. 5 (c) shows the simulated and measured transform function $|S_{21}|$ of two fabricated antennas when are located face-to-face at 80 mm distance far away from each other in the coupling liquid. An Investigation on the $|S_{21}|$ results shows that the transform function of the antenna is almost flat across the required frequency range. However, the slight difference between the simulated and measured results of $|S_{11}|$ and $|S_{21}|$ may be due to the omission of the SMA feed in the simulation environment.

The simulated near-field performance of the proposed antenna, radiating into the loaded open space filled with the coupling medium can be seen in Fig. 6. In order to evaluate the near-field radiation characteristics, the normalized E_y component is sampled at points along arcs with radius 50 mm from the center of the top radiating patch of the antenna. As shown in Fig. 6, the H-plane pattern is radiated symmetrical with respect to the boresight direction (0°) with 6-dB beamwidth for approximately around 60°, whereas the E-plane is developed a squint from 9 to 13.5 GHz, this may be due to the asymmetrical structure of the antenna at that plane and hence changing the radiation mode. In addition, the simulated electric field patterns of the antenna at different frequencies are displayed in Fig. 7. The E_y field as the dominant component at the E-plane of the antenna is monitored in this simulation. As is observed in Fig. 7, the field produced by the antenna is radiated directly to the coupling medium at all 3, 6, 9, and 12 GHz frequencies.

D. ARRAY CONFIGURATION

The simulation setup of the proposed breast cancer imaging system is shown in Fig. 8. In the simulation environment, we selected a hemispherical ceramic shell with the thickness of $T_c = 5$ mm regarding Fig. 1. Also, the modified breast model (see Fig. 3) is fitted into a $R_h = 60$ mm hemispherical breast housing (see Fig. 1) while the center point of the breast housing is considered as the origin of the proposed system. The proposed antenna array consisting of thirty-seven cavity-backed LP-ASP is formed around a 70 mm radius hemisphere regarding the origin of the proposed system. Therefore, the antenna elements will be placed 5 mm far away from the surface of the ceramic shell which can be inserted

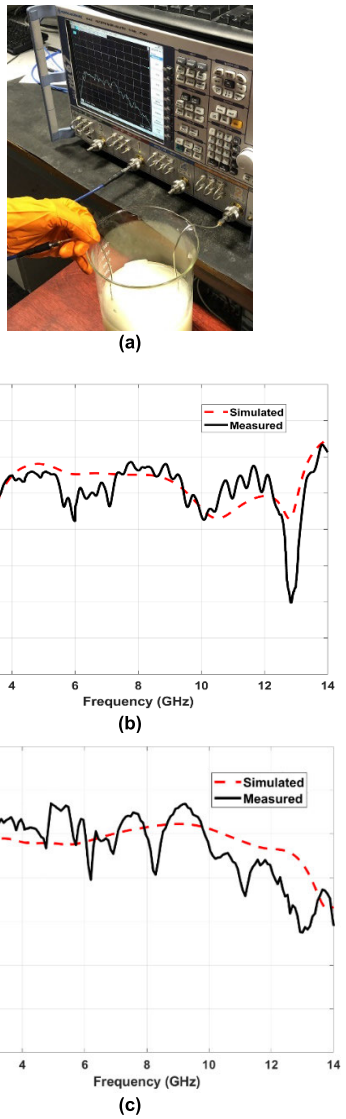

FIGURE 5. The simulated and measured return loss and transform function characteristic of the proposed antenna in the coupling liquid. (a) Measurement setup (b) Return loss, (c) Transform function, $|S_{21}|$.

into the plastic antenna housing in the measurement setup (see Fig. 1). The reason behind the selection of this number of elements is that we have an acceptable number of elements in a symmetric configuration array regarding the size of the proposed elements and their distances from the constructed breast. The top view of antenna array arrangement around the hemispherical ceramic shell is shown in Fig. 8 (b). As shown in the figure, the elements of the array are arranged on three rows (rings) and one antenna located at the top of the hemispherical ceramic. The difference angel between two rows with respect to the origin of the system is chosen to be 25°, whereas the difference angle of adjacent element in each ring is selected different from another regarding the self-central points, as that of the first ring is 30°, the second ring is 15°, and the third ring is 22.5°. It must be noted that, antenna elements are arranged in this configuration to obtain the lowest polarization losses between the elements.

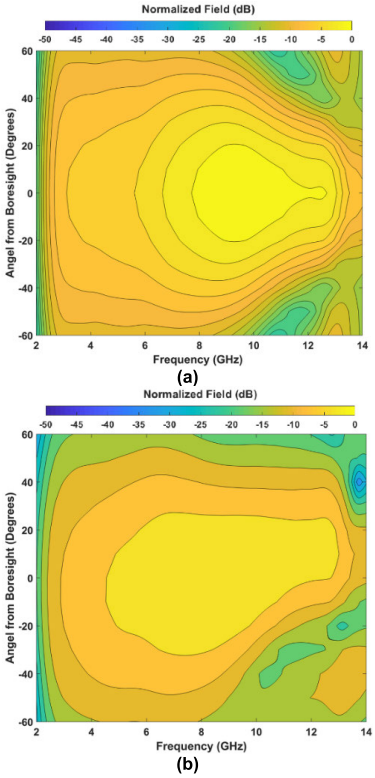

FIGURE 6. The simulated near-field radiation pattern of the proposed antenna inside the matching medium. (a) E-plane, and (b) H-plane.

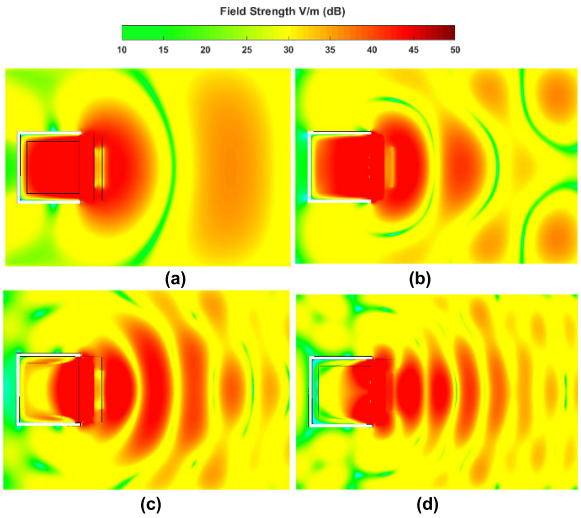

FIGURE 7. A cross section (xz plane) view at the E-plane of the proposed antenna showing, the magnitude distribution of E_y-polarized fields which are produced by the antenna at (a) 3 GHz, (b) 6 GHz, (c) 9 GHz, and (d) 12 GHz.

Additionally, the background of the simulation environment is set as a coupling/matching medium while the permittivity of the low-loss ceramic shell is selected $\varepsilon = 10$ according to [19].

III. PROPOSED ARTIFACT CALIBRATION AND IMAGING METHODS

As mentioned in section I, before applying any beamforming algorithm, the skin reflection and mutual coupling in all

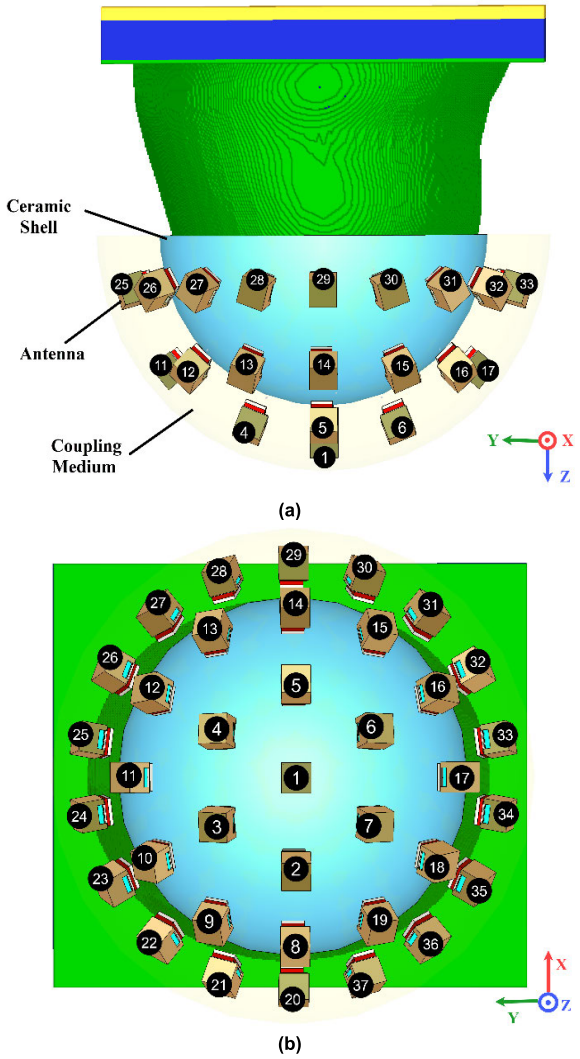

FIGURE 8. The simulation setup of the proposed breast cancer imaging system and the configuration of thirty-seven elements array around the hemispherical ceramic shell (a) Side view (b) Top view.

transmission signal channels must be suppressed. This step is called skin calibration preprocessing.

The proposed imaging method using a hybrid artifact suppression (HAS) technique is outlined in the block diagram of Fig. 9. In order to increase acquired data, the array is rotated around the z-axis. With N elements (N=37) array, a number of available monostatic and bi-static time-domain signals will be $M \times N$ and $M(N \times (N-1))/2$, respectively for M scans. Let us consider the recorded time signal at ith receiver antenna $(Rx)_i$, be denoted by $b_{i,j}(t)$, where j is the number of Tx antenna $(Tx)_j$, i = 1, …, N, j = 1, …, N. Therefore, $b_{i,j,m}(t)$ indicates the mentioned signals at mth scan array.

As shown in Fig. 9, after acquiring the total recorded signals, a signal grouping based on the similarity artifacts in all transmission channels is employed in the first step. Commonly, one group signal is formed through determining a high normalized cross-correlation (NCC) threshold [70], denoted by b_{ncc}, between the recorded signals. Therefore, the

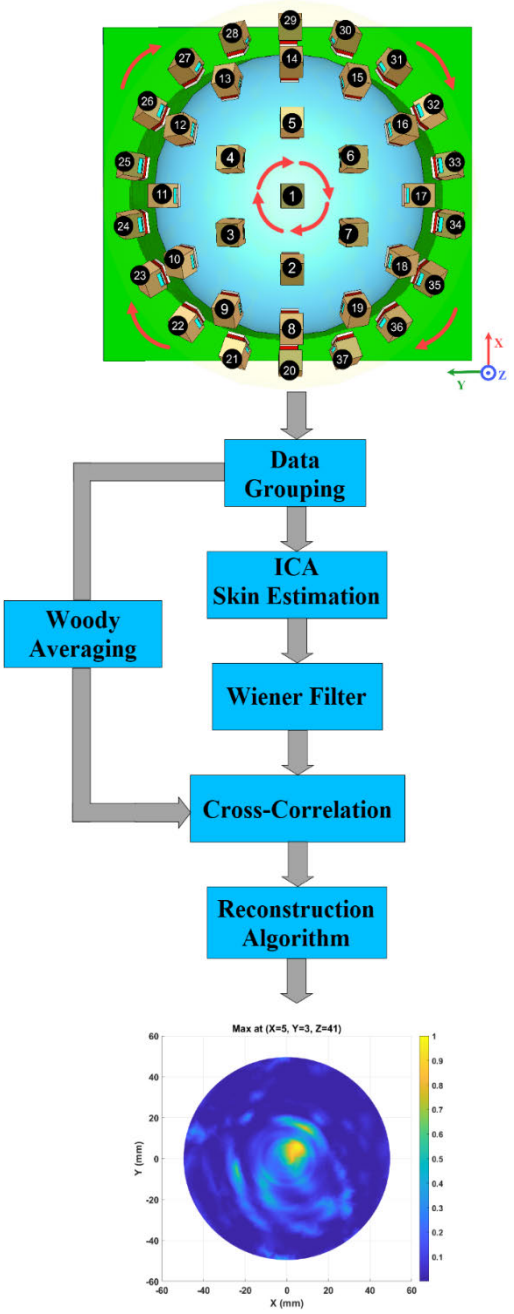

FIGURE 9. The block diagram of the proposed breast cancer imaging system.

monostatic signals can be collected into one group, whereas the bi-static ones form several groups because of the variation distance and polarization between Tx and Rx antennas. As a result, a data grouping matrix $X_{i,j}$, consisting of the monostatic ($b_{i,i,m}$) and bi-static ($b_{i,j,m}$) data can be formed. A number of elements in one matrix group may be different from another since other Tx-Rx signal channels may exhibit similar artifacts relative to that group.

The estimating time location of skin response is performed in the second step. Let assume each signal data within one group be a linear mixture of non-Gaussian sources and independent components. Hence by seeking a linear combination of the signal data which maximizes the non-Gaussianity, we can extract the skin response in the early-stage of the time recorded signals. The determination of non-Gaussianity may be based on negentropy, kurtosis, skewness, and others [71]. Therefore, to estimate the skin response, first, the recorded signals of each group *sphered* using Principal Component Analysis (PCA). Then, the sphered signals ($\hat{X}$) in one group modeled as a linear mixture of sources,

$$\hat{X} = AS \tag{1}$$

where $[A]_{k\times p}$ is defined as a mixing matrix, and $[\mathrm{S}]_{p\times 1}$ described as unknown p ($p \leq k$) sources matrix which must be extracted. Therefore, to recover the p sources, the acquired data will be multiplied by an un-mixing matrix:

$$S = W^T \hat{X} \tag{2}$$

where the un-mixing matrix (W) is the inverse of A and is calculated using the FastICA based on Newton's iteration as the following algorithm:

$$\begin{aligned} &1)\ \text{Choose an initial (e.g. random) weight vector } w.\\ &2)\ \text{Let } w^+ = E\left\{\hat{x}g(w^T\hat{x})\right\} - E\left\{g'(w^T\hat{x})\right\} w\\ &3)\ \text{Let } w = \frac{w^+}{\left\|w^+\right\|}\\ &4)\ \text{If not converged, go back to (2)} \end{aligned} \tag{3}$$

where w is a column of W, $\hat{x}$ is the *vectorized* representation of $\hat{X}$, E is the expected value and g is the derivative of the contrast function G, which is given in [71]. To prevent converging of several vectors to the same solution, we decorrelate output $w_1^T x$, $w_2^T x$, …, $w_n^T x$ at each iteration using a deflation scheme based on Gram Schmidt method [71]. Finally, to extract the skin response of one signal, a cross-correlation is employed between that signal and the obtained sources in the matrix S.

The third step of the proposed calibration method is to apply the Wiener filter algorithm over the estimated artifact time signal in the second step, as illustrated in Fig. 9. In this step, all recorded signals are converted to a sampled waveform, $b_{i,j,m}[n]$. Considering that there are a number of K signals in one group, to remove the artifact at nth sample from kth signal within that group $x_k[n]$, it is estimated from a window $\boldsymbol{x}_k\,[n]$ of length $(2J+1)$ centered on the nth sample in each other *K-1* recorded signals:

$$\boldsymbol{x}_k\,[n] = [x_k\,[\text{n-J}], \ldots, x_k\,[n], \ldots, x_k\,[n+J]]^T \tag{4}$$

where J is the number of samples on either side of nth time sample. Consider the concatenation of all other similar data within one group be defined as

$$\boldsymbol{x}_{2N}[n] = [x_1^T\,[\text{n-J}], \ldots, x_{k-1}^T[n], x_{k+1}^T[n] \ldots, x_N^T[n+J]] \tag{5}$$

Finally, the Wiener filter weights vector $\boldsymbol{q}$ to minimize the mean square error (MSE) over the part of the artifact signal are calculated as [7], [20]

$$\boldsymbol{q} = \arg\min_{q} \sum_{n=n_l}^{n_u} \left| x_k\,[n] - \boldsymbol{q}^T \boldsymbol{x}_{2N}\,[n] \right|^2 \tag{6}$$

where n_l and n_u represent the lower and upper boundaries of skin response, which have been determined by defining a difference threshold between the original and ICA. The solution of the minimization equation (6) is given by [72]. Consequently, the skin subtracted signal $y_k\,[n]$ can be achieved by:

$$y_k\,[n] = x_k[n] - \boldsymbol{q}^T \boldsymbol{x}_{2N}\,[n] \tag{7}$$

In the fourth step, a cross-correlation processing between the Woody averaging's calibrated signals and Wiener filter's is employed to align the filtered out tumor signals which obtained in third step.

In the final step of the proposed method, a Delay-And-Sum (DAS) beamforming as Reconstruction Algorithm is applied to obtain the multi-static images [31] as follow:

$$I\left(P_f\right) = \int_{t=0}^{t=\tau_p} \left[\sum_{k=1}^{K} w_k Y_k(t - \tau(P_f)) \right]^2 dt \tag{8}$$

where $I\left(P_f\right)$ specifies the energy of each scanning focal points, P_f inside of imaging area (the breast), $\tau(P_f)$ is the time-delay corresponding to each focal point, which is determined based on the approximated wave speed in the breast [73], w_k is applied as a weighting factor for compensation of path-dependent attenuation along Tx-Rx paths, τ_p is the integration window which is usually considered a percentage of the input pulse width, and K is the total number of available time-domain calibrated signals Y_k.

It must be noted that the proposed calibration method can be used with any beamformer has been proposed in literatures [28]–[31].

IV. RESULTS AND DISCUSSION

In order to validate the practicality of the proposed calibration method by using of the designed conformal array, a small size single tumor is inserted into the modified breast model (see Fig. 3); then the ability of target detection at near to the skin tissue and on the axis of rotation using the presented HAS method is compared with the most common practical algorithms of calibration such as the Woody averaging, Wiener filter, and Differential rotation methods. The Ideal calibration algorithm is considered as a benchmark to compare the efficiency of the investigated methods.

In scenario I, a 5 mm diameter spherical tumor is located at a position (x=50 mm, y=70 mm, z=105 mm) close to the skin tissue of the modified breast model (see Fig. 3) which is mapped to (x=30 mm, y=20 mm, z=30 mm) regarding the origin of the coordinate system in the simulation setup (see Fig. 8). To increase the similar recorded data, the fixed-array is rotated around z-axis from 0° to 120° with a step size

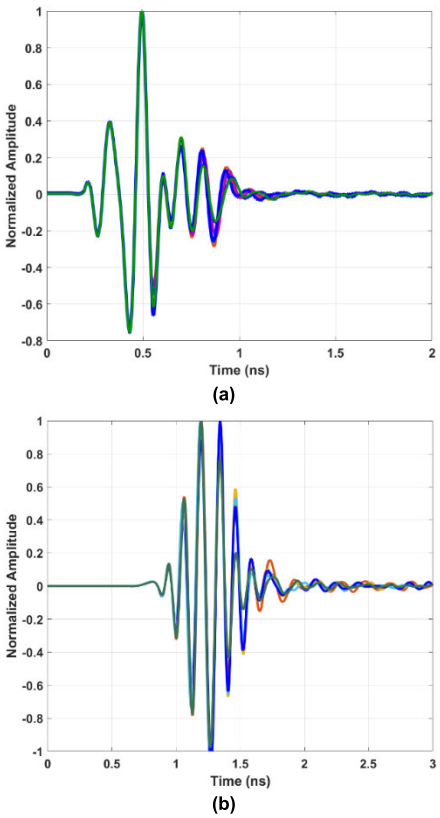

FIGURE 10. Examples of grouped signals which are obtained by a high-value normalized cross-correlation of $b_{ncc} \geq 0.98$, (a) Monostatic (b) Bi-static.

of 15° (M=9 scans). The examples of grouped signals for monostatic and bi-static channels by a high-value normalized cross-correlation ($b_{ncc} \geq 0.98$) are illustrated in Fig. 10. As shown in the figure, the grouped signals experience similar artifact effects in the early-stage. The estimated time range of skin response using ICA is shown as a white window in the first column of Fig. 11 for three cases of recorded signals $b_{6,12}(t)$, $b_{1,5}(t)$ and $b_{5,33}(t)$ in scenario I. Also, the tumor response using the Ideal, Woody averaging, and Wiener filter calibration methods are demonstrated in the yellow window of Figs. 11 (b), (e), and (h). As shown in these figures, the time location of tumor response is detected with an acceptable accuracy using the Woody averaging. However, the time location of the breast tumor response cannot be extracted accurately by the Wiener filter as the mixed tumor response in the late-stage of recorded multi-static signals is filtered out in some channels; nevertheless, the skin removal process is carried out more efficiently in comparison with that of the Woody averaging method. Therefore, a cross-correlation processing between the Wiener filter method and Woody averaging technique is performed to compensate the time delays related to Wiener filter. The extracted tumor response in all three cases of the recorded signals using the proposed HAS method compared with the Woody averaging and Wiener filter calibration methods are shown in Figs. 11 (c), (f), and (i). In addition to previous scenario, to justify the usefulness of

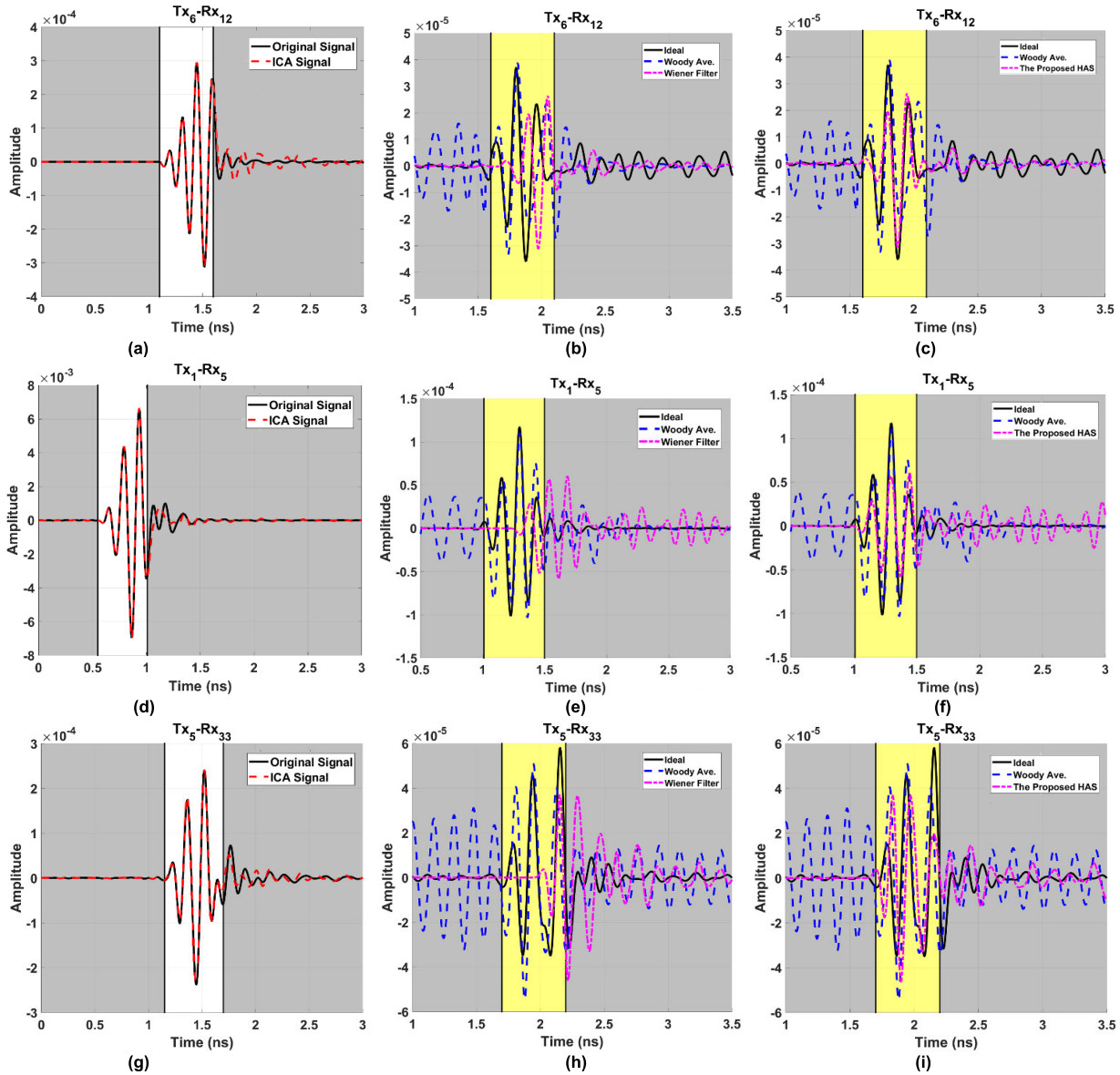

FIGURE 11. The skin removal and extracting tumor responses processing for the modified phantom with a single tumor target at (x = 30 mm, y = 20 mm, z = 30 mm) in the simulation coordinate system (close to the skin tissue of the modified breast model). The time-domain range estimation of skin effect using ICA are shown in (a), (d), and (g) in the white window for $b_{6,12}(t)$, $b_{1,5}(t)$ and $b_{5,33}(t)$ channel signals, respectively. The comparison results of extracted tumor responses between the Woody averaging, Wiener filter, and Ideal calibration methods are illustrated in (b), (e), and (h) in the yellow region corresponding to each recorded signal. The results of the proposed technique for extracting the target response through cross-correlation processing between the Woody averaging and Wiener filter calibration methods in comparison with the Ideal calibration method are demonstrated in (c), (f), and (i).

the HAS algorithm to detect the target, the previous tumor is placed at (x=40 mm, y=88 mm, z=76.5 mm) inside of the modified breast model in scenario II, which will be located at (x=0 mm, y=0 mm, z=40 mm) on the axis of rotation in the simulation coordinate system (see Fig. 8).

The 2D and 3D reconstructed images for scenario I, II using the Ideal, Woody averaging, Differential rotation and the proposed HAS methods are demonstrated in Figs. 12 and 13. Concerning to these images, the consequent peak energy of the proposed HAS technique in both scenarios I and II is closer to tumor location in comparison to Woody averaging method, while the location of the tumor is not detected by the Differential rotation. Also, the energy amount of the proposed HAS method at tumor area is higher than the other regions, while some unwanted clutters exist in the energy profile of the Woody averaging method. As a result, from the reconstructed images, it can be seen the performance of the proposed HAS technique to detect the tumor is more similar to that of the Ideal calibration method compared to the other algorithms.

Quantitative metrics result of the proposed HAS method in comparison with the Ideal and Woody averaging, and the Differential rotation methods for the scenario I and II

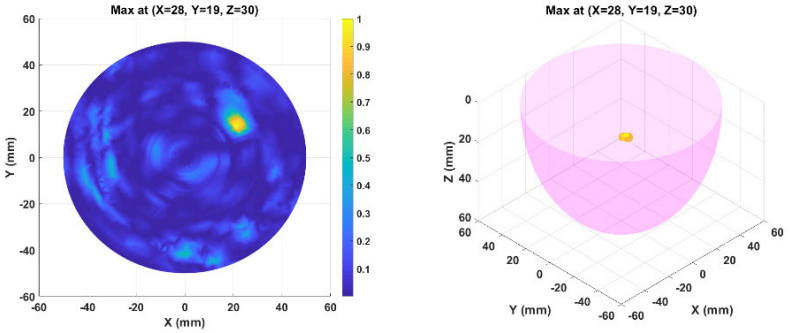

(a)

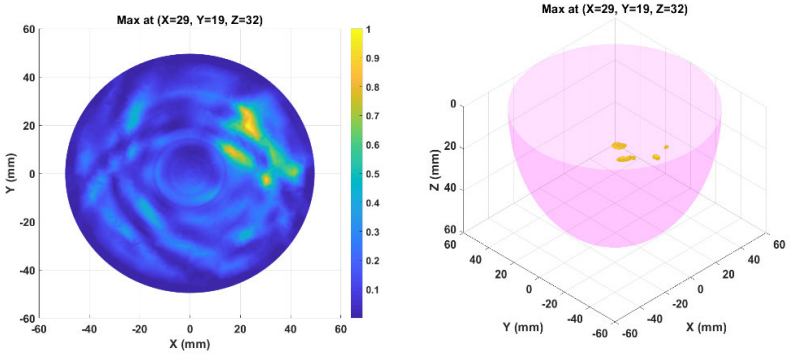

(b)

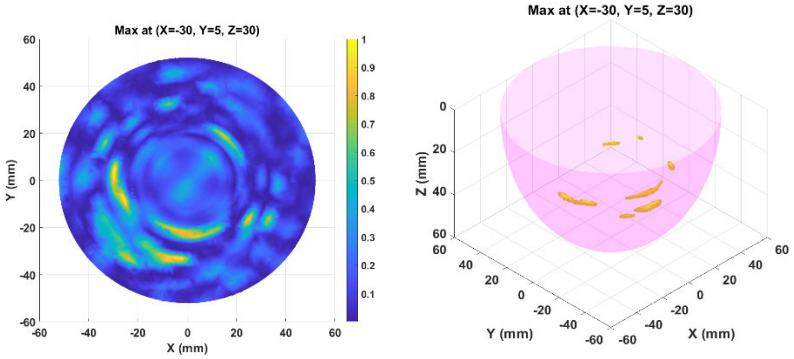

(c)

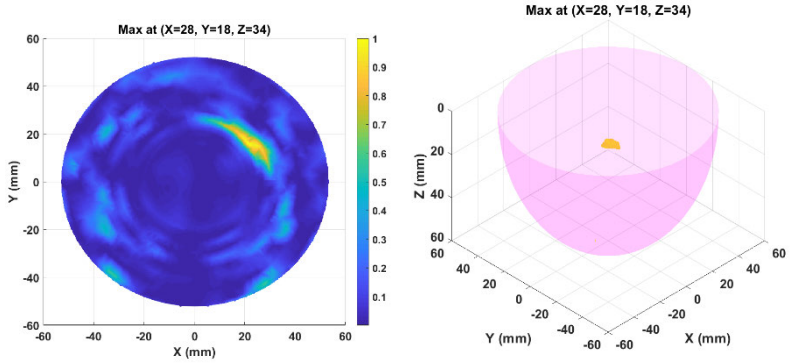

(d)

FIGURE 12. The 2D and 3D reconstructed images for a tumor target which is located at (x=30 mm, y = 20 mm, z = 30 mm) in the simulation coordinate system (close to the skin tissue of the modified breast model), (a) Ideal, (b) Woody averaging, (c) Differential Rotation, and (d) The proposed HAS method.

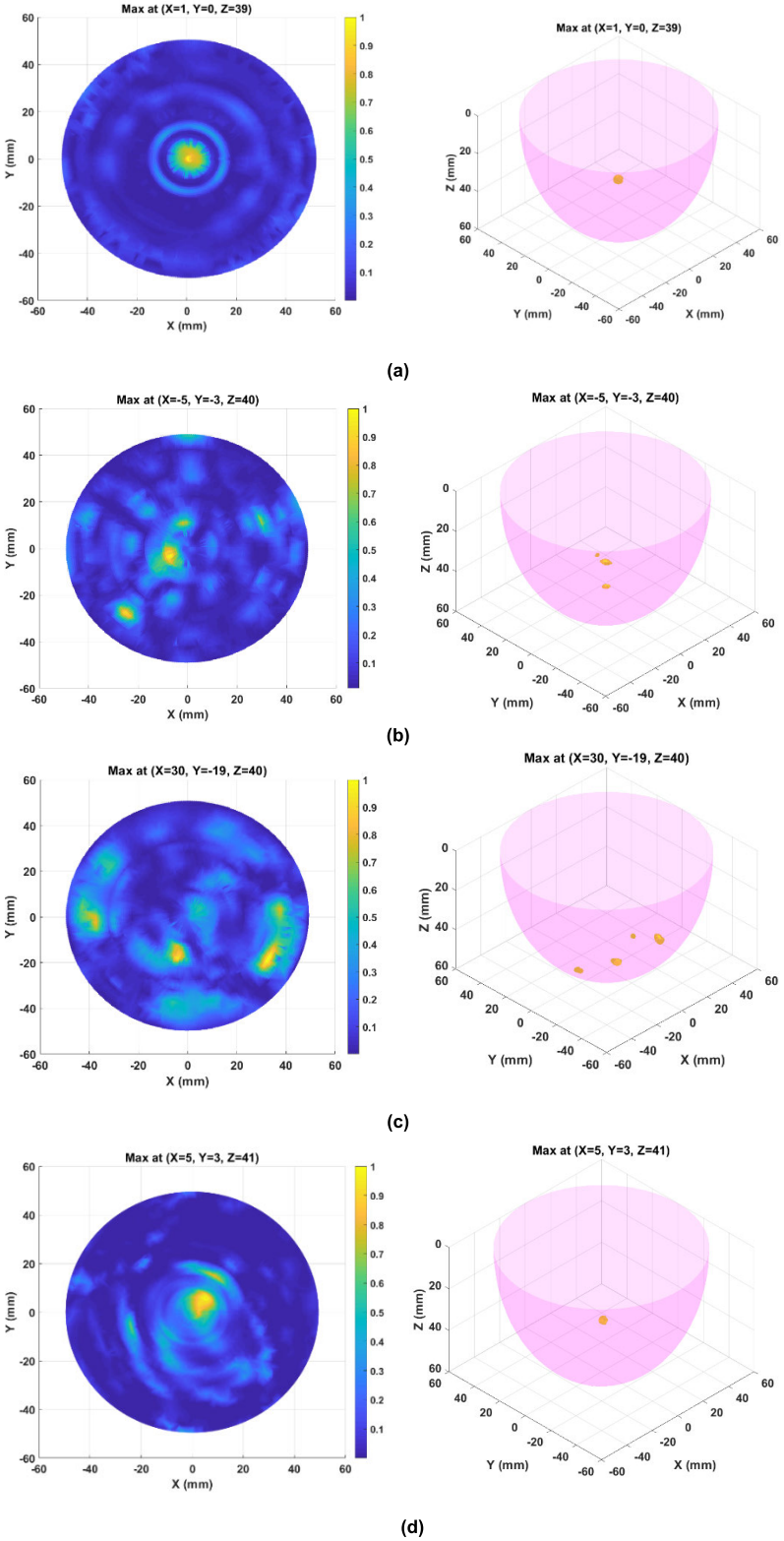

FIGURE 13. The 2D and 3D reconstructed images for a tumor target which is located at (x = 0 mm, y = 0 mm, z = 40 mm) on the axis of rotation in the simulation coordinate system, (a) Ideal, (b) Woody averaging, (c) Differential rotation, and (d) The proposed HAS method.

are listed in Table 2 and 3, respectively. A Signal/Mean Ratio (SMR) is used to compare the mean energy over the tumor area to the average one over the whole breast tissues. And a Signal/Clutter Ratio (SCR) is specified as the peak

TABLE 2. Quantitative metrics result for scenario I.

Method	Detection?	SMR (dB)	SCR (dB)
Ideal	Yes	11.2	2.21
Woody Ave.	Yes	8.43	2.01
Differential Rot.	No	-	-
Proposed HAS	Yes	11.02	2.23

TABLE 3. Quantitative metrics result for scenario II.

Method	Detection?	SMR (dB)	SCR (dB)
Ideal	Yes	9.65	2.19
Woody Ave.	Yes	7.91	1.92
Differential Rot.	No	-	-
Proposed HAS	Yes	9.1	2.02

energy of the tumor area to the peak one of clutter in the imaging region [7], [19].

V. CONCLUSION

This paper presents a hemispherical robust breast cancer imaging system using mutli-static radar approach for a realistic breast model with a non-uniform skin thickness. A conformal array was applied while a cavity-backed low-profile ASP (LP-ASP) antenna designed and used as a unit cell of the array. The proposed antenna has a compact size and high fractional bandwidth which can be deployed around the breast phantom with a large number of elements. In addition, in order to suppress the skin artifact of the breast model, a Hybrid Artifact Suppression (HAS) method was presented. In this calibration method, the skin effect is estimated by ICA and its suppression performed using the Wiener filter. The results of calibrated signals using the Wiener filter technique showed the tumor response is filtered out in some multi-static channels unlike those of calibrated signals by the Woody averaging method, therefore, to compensate the time-delays corresponding to the Wiener filter response, an additional time alignment based on cross-correlation between the calibrated signals of the Woody averaging and wiener filter is employed. Consequently, the imaging results showed that the clutter image can be reduced extremely using the HAS proposed calibration method. As a result, the quantitative metrics of the HAS calibration method proved that the proposed calibration algorithm has a performance similar to the Ideal method and can be a good candidate to detect a small size of cancerous tumors.

REFERENCES

[1] *Breast Cancer, Facts & Figures 2018-2019*. Accessed: 2019. [Online]. Available: https://www.cancer.org

[2] J. G. Elmore and M. B. Barton, "Ten-year risk of false positive screening mammograms and clinical breast examinations," *New England J. Med.*, vol. 338, no. 16, pp. 1089–1096, 1998.

[3] I. C. H. Sharyl, J. Nass, and J. C. Lashof, *Mammography and Beyond: Developing Technologies for the Early Detection of Breast Cancer*. Washington, DC, USA: National Academies Press, 2001.

[4] S. C. Hagness, A. Taflove, and J. E. Bridges, "Two-dimensional FDTD analysis of a pulsed microwave confocal system for breast cancer detection: fixed-focus and antenna-array sensors," *IEEE Trans. Biomed. Eng.*, vol. 45, no. 12, pp. 1470–1479, 1998.

[5] S. P. Poplack, T. D. Tosteson, W. A. Wells, B. W. Pogue, P. M. Meaney, A. Hartov, C. A. Kogel, S. K. Soho, J. J. Gibson, and K. D. Paulsen, "Electromagnetic breast imaging: Results of a pilot study in women with abnormal mammograms," *Radiology*, vol. 243, no. 2, pp. 350–359, May 2007.

[6] E. C. Fear and M. A. Stuchly, "Microwave detection of breast cancer," *IEEE Trans. Microw. Theory Techn.*, vol. 48, no. 11, pp. 1854–1863, Nov. 2000.

[7] X. Li, S. K. Davis, S. C. Hagness, D. W. vanderWeide, and B. D. Vanveen, "Microwave imaging via Space–Time beamforming: Experimental investigation of tumor detection in multilayer breast phantoms," *IEEE Trans. Microw. Theory Techn.*, vol. 52, no. 8, pp. 1856–1865, Aug. 2004.

[8] E. C. Fear, J. Bourqui, C. Curtis, D. Mew, B. Docktor, and C. Romano, "Microwave breast imaging with a monostatic radar-based system: A study of application to patients," *IEEE Trans. Microw. Theory Techn.*, vol. 61, no. 5, pp. 2119–2128, May 2013.

[9] Y. Wang, A. M. Abbosh, B. Henin, and P. T. Nguyen, "Synthetic bandwidth radar for ultra-wideband microwave imaging systems," *IEEE Trans. Antennas Propag.*, vol. 62, no. 2, pp. 698–705, Feb. 2014.

[10] S. C. Hagness, E. C. Fear, and A. Massa, "Guest editorial: Special cluster on microwave medical imaging," *IEEE Antennas Wireless Propag. Lett.*, vol. 11, pp. 1592–1597, 2012.

[11] R. Nilavalan, "Numerical investigation of breast tumour detection using multi-static radar," *IEE Electron. Lett.*, vol. 39, no. 25, pp. 1787–1789, Dec. 2003.

[12] I. Craddock, R. Nilavalan, J. Leendertz, and A. P. R. Benjamin, "Experimental investigation of real aperture synthetically organised radar for breast cancer detection," in *Proc. IEEE Antennas Propag. Soc. Int. Symp.*, vol. 1, Jul. 2005, pp. 179–182.

[13] B. Maklad and E. C. Fear, "Reduction of skin reflections in radar-based microwave breast imaging," in *Proc. 30th Annu. Int. Conf. IEEE Eng. Med. Biol. Soc.*, Aug. 2008, pp. 21–24.

[14] M. Lazebnik, D. Popovic, L. McCartney, C. B. Watkins, M. J. Lindstrom, J. Harter, S. Sewall, T. Ogilvie, A. Magliocco, T. M. Breslin, W. Temple, D. Mew, J. H. Booske, M. Okoniewski, and S. C. Hagness, "A large-scale study of the ultrawideband microwave dielectric properties of normal, benign and malignant breast tissues obtained from cancer surgeries," *Phys. Med. Biol.*, vol. 52, no. 20, pp. 6093–6115, Oct. 2007.

[15] J. C. Y. Lai, "UWB microwave imaging for breast cancer detection—Experiments with heterogeneous breast phantoms," *Prog. Electromagn. Res. M*, vol. 16, pp. 19–29, 2011.

[16] E. C. Fear, X. Li, S. C. Hagness, and M. A. Stuchly, "Confocal microwave imaging for breast cancer detection: Localization of tumors in three dimensions," *IEEE Trans. Biomed. Eng.*, vol. 49, no. 8, pp. 812–822, Aug. 2002.

[17] E. G. Fear and J. M. Sill, "Preliminary investigations of tissue sensing adaptive radar for breast tumor detection," in *Proc. 25th Annu. Int. Conf. IEEE Eng. Med. Biol. Soc.*, vol. 4, Sep. 2003, pp. 3787–3790.

[18] C. D. Woody, "Characterization of an adaptive filter for the analysis of variable latency neuroelectric signals," *Med. Biol. Eng.*, vol. 5, no. 6, pp. 539–554, Nov. 1967.

[19] M. Klemm, J. Leendertz, D. Gibbins, I. Craddock, A. Preece, and R. Benjamin, "Microwave radar-based differential breast cancer imaging: Imaging in homogeneous breast phantoms and low contrast scenarios," *IEEE Trans. Antennas Propag.*, vol. 58, no. 7, pp. 2337–2344, Jul. 2010.

[20] M. O'Halloran, E. Jones, and M. Glavin, "Quasi-multistatic MIST beamforming for the early detection of breast cancer," *IEEE Trans. Biomed. Eng.*, vol. 57, no. 4, pp. 830–840, Apr. 2010.

[21] J. M. Sill and E. C. Fear, "Tissue sensing adaptive radar for breast cancer Detection—Experimental investigation of simple tumor models," *IEEE Trans. Microw. Theory Techn.*, vol. 53, no. 11, pp. 3312–3319, Nov. 2005.

[22] B. Maklad, C. Curtis, E. C. Fear, and G. G. Messier, "Neighborhood-based algorithm to facilitate the reduction of skin reflections in radar-based microwave imaging," *Prog. Electromagn. Res. B*, vol. 39, pp. 115–139, 2012.

[23] D. Byrne, M. O'Halloran, M. Glavin, and E. Jones, "Breast cancer detection based on differential ultrawideband microwave radar," *Prog. Electromagn. Res. M*, vol. 20, pp. 231–242, 2011.

[24] W. Zhi and F. Chin, "Entropy-based time window for artifact removal in UWB imaging of breast cancer detection," *IEEE Signal Process. Lett.*, vol. 13, no. 10, pp. 585–588, Oct. 2006.

[25] M. A. Elahi, A. Shahzad, M. Glavin, E. Jones, and M. O'Halloran, "Hybrid artifact removal for confocal microwave breast imaging," *IEEE Antennas Wireless Propag. Lett.*, vol. 13, pp. 149–152, 2014.
[26] M. A. Elahi, M. Glavin, E. Jones, and M. O'Halloran, "Adaptive artifact removal for selective multistatic microwave breast imaging signals," *Biomed. Signal Process. Control*, vol. 34, pp. 93–100, Apr. 2017.
[27] D. Byrne, M. Sarafianou, and I. J. Craddock, "Compound radar approach for breast imaging," *IEEE Trans. Biomed. Eng.*, vol. 64, no. 1, pp. 40–51, Jan. 2017.
[28] M. Klemm, I. J. Craddock, J. A. Leendertz, A. Preece, and R. Benjamin, "Radar-based breast cancer detection using a hemispherical antenna Array—Experimental results," *IEEE Trans. Antennas Propag.*, vol. 57, no. 6, pp. 1692–1704, Jun. 2009.
[29] D. Byrne and I. J. Craddock, "Time-domain wideband adaptive beamforming for radar breast imaging," *IEEE Trans. Antennas Propag.*, vol. 63, no. 4, pp. 1725–1735, Apr. 2015.
[30] M. Klemm, I. J. Craddock, J. A. Leendertz, A. Preece, and R. Benjamin, "Improved delay-and-sum beamforming algorithm for breast cancer detection," *Int. J. Antennas Propag.*, vol. 2008, Jun. 2008, Art. no. 761402.
[31] R. C. Conceicao, J. J. Mohr, and M. O'Halloran, *An Introduction to Microwave Imaging for Breast Cancer Detection* (Springer Biomedical Engineering). 2016.
[32] D. O'Loughlin, M. O'Halloran, B. M. Moloney, M. Glavin, E. Jones, and M. A. Elahi, "Microwave breast imaging: Clinical advances and remaining challenges," *IEEE Trans. Biomed. Eng.*, vol. 65, no. 11, pp. 2580–2590, Nov. 2018.
[33] R. Benny, T. A. Anjit, and P. Mythili, "An overview of microwave imaging for breast tumor detection," *Prog. Electromagn. Res. B*, vol. 87, pp. 61–91, 2020.
[34] W. Shao and T. McCollough, "Advances in microwave near-field imaging: Prototypes, systems, and applications," *IEEE Microw. Mag.*, vol. 21, no. 5, pp. 94–119, May 2020.
[35] K. D. Paulsen, S. P. Poplack, D. Li, M. W. Fanning, and P. M. Meaney, "A clinical prototype for active microwave imaging of the breast," *IEEE Trans. Microw. Theory Techn.*, vol. 48, no. 11, pp. 1841–1853, Nov. 2000.
[36] S. P. Poplack, K. D. Paulsen, A. Hartov, P. M. Meaney, B. W. Pogue, T. D. Tosteson, M. R. Grove, S. K. Soho, and W. A. Wells, "Electromagnetic breast imaging: Average tissue property values in women with negative clinical findings," *Radiology*, vol. 231, no. 2, pp. 571–580, May 2004.
[37] P. M. Meaney, P. A. Kaufman, L. S. Muffly, M. Click, S. P. Poplack, W. A. Wells, G. N. Schwartz, R. M. di Florio-Alexander, T. D. Tosteson, Z. Li, S. D. Geimer, M. W. Fanning, T. Zhou, N. R. Epstein, and K. D. Paulsen, "Microwave imaging for neoadjuvant chemotherapy monitoring: Initial clinical experience," *Breast Cancer Res.*, vol. 15, no. 2, pp. 1–16, Apr. 2013.
[38] M. Klemm, I. J. Craddock, and J. A. Leendertz, "Clinical trials of a UWB imaging radar for breast cancer," in *Proc. 4th Eur. Conf. Antennas Propag.*, Barcelona, Spain, Apr. 2010, pp. 1–4.
[39] H. Massey, N. Ridley, I. Lyburn, L. Jones, S. Taylor, M. S. Lewis, P. Bannister, and M. Shere, "Radiowave detection of breast cancer in the symptomatic clinic—A multi-centre study," in *Proc. Int. Cambridge Conf. Breast Imag.*, Cambridge, U.K., 2017, pp. 3–4.
[40] A. W. Preece, I. Craddock, M. Shere, L. Jones, and H. L. Winton, "MARIA m4: Clinical evaluation of a prototype ultrawideband radar scanner for breast cancer detection," *J. Med. Imag.*, vol. 3, no. 3, Jul. 2016, Art. no. 033502.
[41] D. Kurrant, J. Bourqui, and E. Fear, "Surface estimation for microwave imaging," *Sensors*, vol. 17, no. 7, p. 1658, Jul. 2017.
[42] E. Porter, H. Bahrami, A. Santorelli, B. Gosselin, L. A. Rusch, and M. Popovic, "A wearable microwave antenna array for time-domain breast tumor screening," *IEEE Trans. Med. Imag.*, vol. 35, no. 6, pp. 1501–1509, Jun. 2016.
[43] E. Porter, M. Coates, and M. Popovic, "An early clinical study of time-domain microwave radar for breast health monitoring," *IEEE Trans. Biomed. Eng.*, vol. 63, no. 3, pp. 530–539, Mar. 2016.
[44] F. Yang, L. Sun, and Z. Hu, "A large-scale clinical trial of radar-based microwave breast imaging for Asian women: Phase I," in *Proc. IEEE Int. Symp. Antennas Propag. USNC/URSI Nat. Radio Sci. Meeting*, San Diego, CA, USA, Jul. 2017, pp. 781–783.
[45] H. Song, S. Sasada, T. Kadoya, "Detectability of breast tumor by a hand-held impulse-radar detector: Performance evaluation and pilot clinical study," *Sci. Rep.*, vol. 7, no. 1, Dec. 201, Art. no. 0163537.
[46] Y. Kuwahara, "Microwave imaging for early breast cancer detection," in *New Perspectives in Breast Imaging*, A. M. Malik, Ed. Rijeka, Croatia: InTech, Oct. 2017.
[47] A. Fasoula, L. Duchesne, J. Gil Cano, P. Lawrence, G. Robin, and J.-G. Bernard, "On-site validation of a microwave breast imaging system, before first patient study," *Diagnostics*, vol. 8, no. 3, p. 53, Aug. 2018.
[48] J. D. Gil Cano, A. Fasoula, L. Duchesne, and J. G. Bernard, "Wavelia Breast Imaging: The Optical Breast Contour Detection Subsystem," *Appl. Sci.*, vol. 10, no. 4, p. 1234, 2020.
[49] ICH GCP Clinical Trials Registry. *Pilot Clinical Evaluation of a Microwave Imaging System for Early Breast Cancer Detection Pilot Clinical Study on a Low-Power Electromagnetic Wave Breast Imaging Device for Cancer Screening Purposes*. Accessed: Jul. 2019. [Online]. Available: https://clinicaltrials.gov/ct2/show/NCT03475992
[50] Micrima-Maria Update. (Jun. 2019). *Micrima Enters into Distribution Agreement With Hologic for its Novel Breast Imaging System MARIA*. Accessed: Jan. 6, 2020. [Online]. Available: https://micrima.com/micrima newsletters/
[51] D. Gibbins, M. Klemm, I. J. Craddock, J. A. Leendertz, A. Preece, and R. Benjamin, "A comparison of a wide-slot and a stacked patch antenna for the purpose of breast cancer detection," *IEEE Trans. Antennas Propag.*, vol. 58, no. 3, pp. 665–674, Mar. 2010.
[52] J. Bourqui, M. Okoniewski, and E. C. Fear, "Balanced antipodal vivaldi antenna with dielectric director for near-field microwave imaging," *IEEE Trans. Antennas Propag.*, vol. 58, no. 7, pp. 2318–2326, Jul. 2010.
[53] T. Sugitani, S. Kubota, A. Toya, X. Xia, and T. Kikkawa, "A compact 4×4 planar UWB antenna array for 3-D breast cancer detection," *IEEE Antennas Wireless Propag. Lett.*, vol. 12, pp. 733–736, 2013.
[54] R. Nilavalan, I. J. Craddock, A. Preece, J. Leendertz, and R. Benjamin, "Wideband microstrip patch antenna design for breast cancer tumour detection," *IET Microw., Antennas Propag.*, vol. 1, no. 2, pp. 277–281, 2007.
[55] Y. Wang, A. E. Fathy, and M. R. Mahfouz, "Novel compact tapered microstrip slot antenna for microwave breast imaging," in *Proc. IEEE Int. Symp. Antennas Propag. (APSURSI)*, Jul. 2011, pp. 2119–2122.
[56] M. Solis Nepote, D. R. Herrera, D. F. Tapia, S. Latif, and S. Pistorius, "A comparison study between horn and Vivaldi antennas for 1.5–6 GHz breast microwave radar imaging," in *Proc. 8th Eur. Conf. Antennas Propag. (EuCAP)*, The Hague, The Netherlands, vol. 2014, pp. 59–62.
[57] M. Jalilvand, X. Li, L. Zwirello, and T. Zwick, "Ultra wideband compact near-field imaging system for breast cancer detection," *IET Microw., Antennas Propag.*, vol. 9, no. 10, pp. 1009–1014, 2015.
[58] M. T. Islam, M. Z. Mahmud, N. Misran, J.-I. Takada, and M. Cho, "Microwave breast phantom measurement system with compact side slotted directional antenna," *IEEE Access*, vol. 5, pp. 5321–5330, 2017.
[59] M. T. Islam, M. Z. Mahmud, M. T. Islam, S. Kibria, and M. Samsuzzaman, "A low cost and portable microwave imaging system for breast tumor detection using UWB directional antenna array," *Sci. Rep.*, vol. 9, no. 1, p. 15491, Dec. 2019.
[60] K. N. Paracha, S. K. Abdul Rahim, P. J. Soh, and M. Khalily, "Wearable antennas: A review of materials, structures, and innovative features for autonomous communication and sensing," *IEEE Access*, vol. 7, pp. 56694–56712, 2019.
[61] P. M. Meaney and K. D. Paulsen, "Addressing multipath signal corruption in microwave tomography and the influence on system design and algorithm," *J. Biomed. Eng. Biosci.*, vol. 1, 1-13, 2018.
[62] (2020). *Evolving Medical Imaging*. [Online]. Available: https://micrima.com
[63] T. Pope, Jr., "Breast skin thickness: Normal range and causes of thickening shown on film-screen mammography," *J. Can. Assoc. Radiol.*, vol. 35, no. 4, pp. 365–368, 1984.
[64] A. Sutradhar and M. J. Miller, "*In vivo* measurement of breast skin elasticity and breast skin thickness," *Skin Res. Technol.*, vol. 19, no. 1, pp. e191–e199, Feb. 2013.
[65] Wisconsin System. (2020). *U. University of Wisconsin cross-disciplinary electromagnetics laboratory@ONLINE*. [Online]. Available: http://uwcem.ece.wisc.edu/ phantomRepository.html
[66] (2020). *Autodesk 3ds Max*. [Online]. Available: https://www.autodesk.com
[67] MATLAB. (2018). *MATLAB program@ONLINE*. [Online]. Available: http://www.mathworks.com/store?s_eid=ppc_29850095842&q=matlab
[68] *CST Microwave Studio*, CST, Framingham, MA, USA, 2019.
[69] T. Henriksson, D. Gibbins, D. Byrne, and I. J. Craddock, "A Liquid with Tunable Dielectric Properties for Wideband Microwave Sensing of Biological Targets," in *Proc. 12th Eurp. Conf. Antennas Propag.*, Apr. 2018, doi: 10.1049/cp.2018.0502.
[70] J. Martin and J. L. Crowley, "Comparison of correlation techniques," in *Proc. Int. Conf. Intell. Auton. Syst.*, Karlsruhe, Germany, 1995, pp. 86–93.

[71] A. Hyvarinen, "Fast and robust fixed-point algorithms for independent component analysis," *IEEE Trans. Neural Netw.*, vol. 10, no. 3, pp. 626–634, May 1999.
[72] S. Haykin, *Adaptive Filter Theory*, 4th ed. Upper Saddle River, NJ, USA: Prentice-Hall, 1996.
[73] M. Sarafianou, "MUSIC processing for permittivity estimation in a Delay-and-Sum imaging system," in *Proc. 7th Eur. Conf. Antennas Propag. (EuCAP)*, Apr. 2013, pp. 839–842.

MEHDI MEHRANPOUR received the B.Sc. degree in electrical engineering from Tabriz University, Tabriz, Iran, and the M.Sc. degree in telecommunication engineering from Urmia University, Urmia, Iran. He is currently pursuing the Ph.D. degree with Imam Khomeini International University, Qazvin, Iran. His research interests include microwave and radar imaging, numerical methods in electromagnetics, phased arrays, antennas and propagation, equivalent circuit models, reconfigurable structures, radar systems, signal processing, and electromagnetic theory. Since 2012, he has been a member of the IEEE Antennas and Wireless Propagation Letters (AWPL) reviewer group.

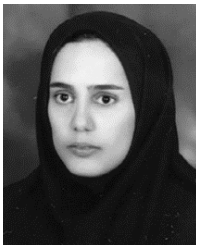

SAUGHAR JARCHI (Member, IEEE) received the B.S. degree in electrical engineering from the Amirkabir University of Technology, Tehran, Iran, and the M.Sc. degree from the University of Tehran, Tehran, and the Ph.D. degree in field and wave communications from the University of Tehran, in 2012. In 2012, she joined the Faculty of Technical and Engineering, Imam Khomeini International University (IKIU), Qazvin, Iran, as an Assistant Professor. Her work background and research interests include metamaterials, metasurfaces, and plasmonics, applications of metamaterials and metasurfaces in antenna enhancement providing compact, wideband and high gain antennas, as well as design of planar and low profile antennas for MIMO and biomedical applications.

ASGHAR KESHTKAR was born in Ardabil, Iran, in 1962. He received the B.Sc. degree in electrical engineering from Tehran University, Tehran, Iran, in 1989, the M.Sc. degree in electrical engineering from the K. N. Toosi University of Technology, Tehran, in 1992, and the Ph.D. degree in electrical engineering from the Iran University of Science and Technology, Tehran, in 1999. He is currently a Professor with the Faculty of Engineering and Technology, Imam Khomeini International University, Qazvin, Iran. His current research interests include electromagnetism, electromagnetic launchers, antennas, and bio-electromagnetism.

AYAZ GHORBANI received the Postgraduate Diploma, M.Phil., and Ph.D. degrees in communication engineering from the University of Bradford, Bradford, U.K., in 1984, 1985, and 1987, respectively. He was on sabbatical leave from the University of Bradford, from 2004 to 2005. Since 1987, he has been teaching various courses at the Department of Electrical Engineering, Amirkabir University of Technology, Tehran, Iran, where he is currently a Professor with the Department of Electrical and Electronic Engineering. He has authored or coauthored more than 180 papers in various journals and different conferences. He also written (in Persian) more than ten books in the field of microwave engineering, radar, electromagnetics, and electromagnetic compatibility. He received the John Robertshaw Travel Award and the URSI Young Scientists Award from Bradford University, in 1987, and the General Assembly of URSI, Prague, Czech Republic, in 1990. He also received the Seventh and Tenth Khwarizmi International Festival Prizes, for design and implementation of an anti-echo chamber and microwave subsystems, in 1993 and 1995, respectively.

ALI ARAGHI (Graduate Student Member, IEEE) received the M.Sc. degree in electrical engineering-telecommunication-wave from Shahed University, Tehran, Iran, in 2012. He is currently pursuing the Ph.D. degree with the Home of the 5G Innovation Centre (5GIC), Institute for Communication Systems (ICS), University of Surrey, U.K. From January 2012 to October 2018, he worked at the Iran Telecommunication Research Centre (ITRC), as a Research Assistant on Antennas and Propagation. His main research interests include leaky-wave structures, holography theory, metasurfaces, large intelligence surfaces, and the theory of characteristic modes.

OKAN YURDUSEVEN (Senior Member, IEEE) received the B.Sc. and M.Sc. degrees in electrical engineering from Yildiz Technical University, Istanbul, Turkey, in 2009 and 2011, respectively, and the Ph.D. degree in electrical engineering from Northumbria University, Newcastle upon Tyne, U.K., in 2014.

From 2018 to 2019, he was a NASA Postdoctoral Fellow at the Jet Propulsion Laboratory, California Institute of Technology, USA. From 2014 to 2018, he was a Postdoctoral Research Associate with the Department of Electrical and Computer Engineering, Duke University, USA. He is currently a Senior Lecturer (Associate Professor) with the School of Electronics, Electrical Engineering and Computer Science, Queen's University Belfast, U.K. He is also an Adjunct Assistant Professor with Duke University, USA. His research interests include microwave and millimeter-wave imaging, multiple-input-multiple-output (MIMO) radar, wireless power transfer, antennas and propagation, antenna measurement techniques, and metamaterials. He has authored more than 100 peer-reviewed technical journal and conference papers.

Dr. Yurduseven is a member of the European Association on Antennas and Propagation (EurAAP). He received the Outstanding Postdoctoral Award from Duke University, in 2017. He was a recipient of the NASA Postdoctoral Program Fellowship administrated by Universities Space Research Association (USRA), in 2018. In 2019, in collaboration with the University of Limoges, France, he received the Alliance Hubert Curien Award funded by the British Council. In 2020, he was bestowed the Leverhulme Trust Research Leadership Award. He has served as a technical program committee member and a guest editor for several conferences and journals in these fields.

MOHSEN KHALILY (Senior Member, IEEE) is currently a Lecturer of Antenna and Propagation with the Home of the 5G Innovation Centre (5GIC), Institute for Communication Systems (ICS), University of Surrey, U.K., where he was a Research Fellow on Antennas and Propagation, from December 2015 to March 2019. Prior to joining the 5GIC, he was a Senior Lecturer with the Wireless Communication Centre (WCC), University Technology Malaysia (UTM). He has published over 100 academic papers in international peer-reviewed journals and conference proceedings. His research interests include surface electromagnetic, large intelligent surface, metasurfaces, dielectric resonator antennas, phased arrays, hybrid beamforming, and mm-wave and terahertz antennas and propagation. He is a Fellow of the U.K. Higher Education Academy, a member of the IEEE Antennas and Propagation Society, the IEEE Communication Society, and the IEEE Microwave Theory and Techniques Society, and an Associate Editor of IEEE Access.